Proceedings of ALGORITMY 2024
pp. 85–98

VECTOR FIELD RECONSTRUCTION FROM SPARSE SAMPLES BY TRIPLE-LAPLACIAN

GIULIA LUPI, KAROL MIKULA

Abstract. We present a mathematical model to reconstruct vector fields from given sparse samples inside the domain. We applied the presented model to reconstruct the velocity vector field driving macrophages toward the wound during wound healing. In this application, the sparse samples are the sparsely distributed velocity vectors given on macrophage trajectories. The method consists of solving a minimization problem, which leads to applying the Laplace equation with suitable boundary conditions to the two components of the vectors and the vector lengths. The values given by sparse samples are the prescribed Dirichlet conditions inside the domain, and we impose zero Neumann boundary conditions on the domain boundary. Solving the Laplace equation, we obtain a smooth vector field in the whole domain. We prove the existence and uniqueness of a weak solution for the considered partial differential equation with mixed boundary conditions, present its numerical solution, and show numerical results.

Key words. Vector field reconstruction, Laplace operator, sparse samples, weak solution

1. Introduction. Reconstruction of vector fields from sparse samples is relevant in several computational contexts, like fluid dynamics visualization, texture synthesis, non-photorealistic rendering, optical flow fields, or map registration [5], [8], [10]. In [8], the authors construct local piecewise polynomial approximations using least squares techniques and combine these approximations through partitions of unity. In [11], the author solves the approximation problem of representing the vector field by combining linearly independent vector fields, called 'basis fields,' which are invariant under coordinate transformations. In [5], the authors developed a model for reconstructing smooth tangent vector fields. Given user-specified constraints, they used an intrinsically coordinate-free approach in which the discrete Laplace operator enforces field smoothness. Laplace interpolation has also been used in image processing tasks, such as image inpainting and image compression [4], [15]. In [10], the authors developed the so-called *Locally Affine Globally Laplace* (LAGL) map transformation. They first designed affine transformations from one map to the other and then solved the Laplace equation to reconstruct the other points of the map smoothly.
The mathematical model we propose to reconstruct the 2D vector field is based on interpolating/extrapolating the given information about the vector field. For this reason, the values given by sparse samples are the Dirichlet conditions inside the domain. Throughout the paper, the term sparse sample will indicate the position and value of the prescribed Dirichlet condition. We apply zero Neumann boundary conditions on the boundary: this choice is again because we do not want to add any new information. We consider the following minimization problem for the two vector components and the vector length

$$\min_u \frac{1}{2} \int_\Omega \|\nabla u\|^2, \tag{1.1}$$

where $u : \Omega \to \mathbb{R}$ is a function defined on $\Omega \subseteq \mathbb{R}^2$ and $E[u] = \frac{1}{2}\int_\Omega \|\nabla u\|^2$ is the Dirichlet energy. Solving (1.1) leads to

$$-\Delta u = 0, \tag{1.2}$$

with appropriate boundary conditions that will be discussed in detail in Section 2. Suppose we use only double-Laplacian [5] for the two vector components. In that case, the direction of the vectors changes smoothly from one to the other, where the vectors influence each other, and it is extrapolated from the Dirichlet conditions, where the vectors do not influence each other. However, it is well known that the Laplace equation averages the neighboring points. Therefore, as already observed in [5], double-Laplacian gives the desired behavior for the vector directions but shortens the vector lengths. Since our approach is based on extracting the vector field from the given information, it is reasonable to consider that the vector length should also be reconstructed starting from the given Dirichlet conditions. For this reason, we consider the same minimization problem (1.1) for the vector lengths. Then, the model for vector field reconstruction by triple-Laplacian consists of solving the Laplace equation 3 times with suitable Dirichlet and Neumann boundary conditions. Namely, considering the two vector components v_x and v_y and the vector length L, we solve

$$-\Delta u^i = 0 \quad i = 1, 2, 3 \tag{1.3}$$

where $u^1 = v_x$, $u^2 = v_y$ and $u^3 = L$.
We applied the presented model to reconstruct the velocity vector field driving macrophages toward the wound during wound healing. In the presence of an injury, macrophages activate in response to danger signals [16]. To reconstruct the velocity vector field caused by the danger signals from videos of macrophages moving toward the wound site, we extracted the trajectories using the method described in [13]. Macrophages often show both random and directional motion: we assume that the gradient of the danger signal causes the drift of macrophage motion toward the wound. Thus, although we do not know the danger signal gradient explicitly, we use the drift part of the macrophage motion to reconstruct the corresponding velocity vector field. To do this, we smooth the trajectories using the model described in [9]. The smoothing algorithm separates the directional part of the motion from the random parts and finds the velocity vectors on the smoothed curves. We use these vectors to define the sparse samples to reconstruct the velocity vector field.
In Section 2, we will derive the model considering the different boundary conditions for triple Laplace equations (1.3) in detail. We will present two different approaches. For the first one, we will prove the existence and uniqueness of a weak solution. For the second approach, we will present theoretical results ensuring the existence of a unique solution under suitable conditions on the domain boundary. In section 3, we will present the problem's numerical solution and show numerical experiments and results on real macrophage data.

2. Mathematical model. Consider $\tilde{\Omega}$ the auxiliary domain and

$$\Gamma^2 = \partial\tilde{\Omega} \tag{2.1}$$

the domain boundary. We define the domain Ω, in which we will solve the Laplace equation, whose boundary is $\partial\Omega = \Gamma^2 \cup \Gamma^1$, where Γ^1 is a set of curves (open or closed depending on the definition) on which the Dirichlet conditions are prescribed. In our specific application, where we find the trajectories starting from videos of macrophages moving, the Dirichlet conditions are defined by velocity vectors on smooth trajectories. We consider the general situation where the sparse samples are given in points. We consider small squares around the given points and prescribe the Dirichlet conditions on the boundary of the squares. The problem's resolution will then give the

size of the squares. To define the model and prove the existence of a unique weak solution, we impose the following conditions: the squares can not touch the domain boundary Γ^2 and can not touch each other.
In Remark 1, we will show a second approach to define the model problem. In this approach, the Dirichlet conditions are prescribed on curves, which are the smooth trajectories in our specific application. Therefore, Γ^1 is the set of smooth open curves. Notice that the mathematical model we propose can cover more general situations. Moreover, it can also cover the second approach if we understand the smooth trajectories as discrete curves.

Let us define the model problem. Let us have a pixel (finite volume) grid coming

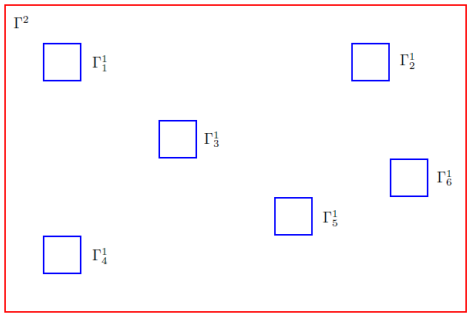

FIG. 2.1. *Example of multiply connected set Ω. We consider small squares given by the pixel grid so that $\Omega = \tilde{\Omega}/S$ remains connected.*

from (e.g. image processing) application. We assume that the sparse sample represents a value given in the pixel's center or a constant value for the whole pixel. In any case, we subdivide the pixel into 9 equal squares and consider the prescribed Dirichlet condition in the central square. This way, the squares will not touch each other, and they will not touch the domain boundary, so we will obtain a domain with Lipschitz boundary, for definition see [14]; an example of such domain is shown in Fig. 2.1. Thus, consider the squares $S_p(k)$ $p = 1, ..., s$, with side's length $k = \frac{h}{3}$, where h is the pixel size. Let us define

$$S = \bigcup_{p=1}^{s} S_p(k), \tag{2.2}$$

and

$$\Gamma^1_p = \partial S_p(k) \quad \forall p = 1, 2, ..., s, \quad \partial S = \Gamma^1 = \bigcup_{p=1}^{s} \Gamma^1_p. \tag{2.3}$$

Indicate by

$$\Omega = \tilde{\Omega}/S, \tag{2.4}$$

so that

$$\partial\Omega = \Gamma^2 \cup \Gamma^1. \tag{2.5}$$

Notice that, due to the choice of k, the set Ω is multiply connected [1]. Therefore, in this case, we will solve the minimization problem in Ω subject to the following boundary conditions

- Zero Neumann boundary conditions on Γ^2

$$\frac{\partial u}{\partial \nu}(x) = 0 \quad x \in \Gamma^2, \tag{2.6}$$

  where ν is the unit outer normal vector to the boundary Γ^2.
- Dirichlet boundary conditions on Γ^1

$$g(x) = g_i \quad x \in \Gamma_i^1 \quad \forall i = 1, 2, ..., s, \tag{2.7}$$

  where $g_i : \Gamma_i^1 \to \mathbb{R}$ gives the value of the sample on the boundary of the square $S_i(k)$.

Solving the variational problem (1.1) with conditions (2.6) and (2.7) is equivalent to finding the solution of the following boundary value problem

$$\begin{cases} -\Delta u(x) = 0, & x \in \Omega, \\ \frac{\partial u}{\partial \nu}(x) = 0, & x \in \Gamma^2, \\ u(x) = g(x), & x \in \Gamma^1. \end{cases} \tag{2.8}$$

In what follows, we will prove the existence and uniqueness of a weak solution for the boundary value problem (2.8). First, let us define the weak solution for our specific case; for a more general theory, see [14].

Definition 2.1. *Let*

$$\Omega \subset \mathbb{R}^2 \tag{2.9}$$

be a domain with a Lipschitz boundary $\Gamma = \Gamma^1 \cup \Gamma^2$*, with* $\Gamma^1 \cap \Gamma^2 = \emptyset$ *and*

$$\Gamma^1 = \bigcup_{p=1}^{s} \Gamma_p^1, \quad \Gamma_p^1 \cap \Gamma_q^1 = \emptyset \ \ \forall p \neq q, \tag{2.10}$$

so that $\Gamma_1^1, ..., \Gamma_s^1, \Gamma^2$ *are disjoint open connected parts of* Γ *of positive measure. Consider the bilinear form*

$$((v, u)) = \int_\Omega \sum_{l=1}^{2} \frac{\partial v}{\partial x_l} \frac{\partial u}{\partial x_l} dx. \tag{2.11}$$

Let be given

$$B_{11}, ..., B_{s1}, \tag{2.12}$$

the operators characterizing the Dirichlet boundary conditions on the individual parts $\Gamma_1^1, ..., \Gamma_s^1$ *of* Γ^1*, and*

$$V = \{v; \ v \in W_2^1(\Omega), \ B_{11}v = 0, ..., B_{s1}v = 0 \text{ on } \Gamma^1 \text{ in the sense of the traces}\}. \tag{2.13}$$

Let be given

$$g_{p1} \in L_2(\Gamma_p^1), \quad p = 1, ..., s, \tag{2.14}$$

and

$$w \in W_2^1(\Omega) \tag{2.15}$$

satisfying on Γ_p^1 $(p = 1, ..., s)$

$$B_{11}w = g_{p1}, ..., B_{s1}w = g_{s1} \tag{2.16}$$

in the sense of the traces. The function $u \in W_2^1(\Omega)$ *is called the weak solution of the boundary value problem given by the data* (2.9)-(2.16) if

$$u - w \in V, \tag{2.17}$$

$$((v, u)) = 0 \quad \forall v \in V. \tag{2.18}$$

For the proof of the existence of a weak solution, we need the Lax Milgram theorem. Thus, the bilinear form must be V-elliptic and bounded [14]. Recall that, given the bilinear form $((v, u))$ and the space V of Def. 2.1, $((v, u))$ is called V-elliptic if there exists a constant $\mu > 0$ such that for every $v \in V$ we have

$$((v, v)) \geq \mu \|v\|_V^2. \tag{2.19}$$

On the other hand, the bilinear form $((v, u))$ is bounded if, for every $v, u \in W_2^1(\Omega)$, there exists a constant $K > 0$ such that

$$|((v, u))| \leq K \|v\|_{W_2^1(\Omega)} \|u\|_{W_2^1(\Omega)}. \tag{2.20}$$

THEOREM 2.2. *The boundary value problem (*2.8*) has exactly one weak solution* $u \in W_2^1(\Omega)$ *in the sense of* Def. 2.1.

Proof. We apply Theorem 33.2 in [14]. It states that given a boundary value problem according to Def. 32.2 in [14], and a bilinear form $((v, u))$ that is V-elliptic and bounded, there exists a unique weak solution of the considered boundary value problem. Therefore, it will be sufficient to prove that: (i) the set Ω has a Lipschitz boundary, (ii) condition (2.14) holds for the function g in (2.7), (iii) it exists w as in Def. 2.1, and (iv) $((v, u))$ is V-elliptic and bounded. Indeed, Def. 2.1 is a specific case of the more general Def. 32.2 in [14], where in our case the function f on the right-hand side of the equation is $f = 0 \in L_2(\Omega)$, and the functions h on the right-hand side of the Neumann boundary conditions is $h = 0 \in L_2(\Omega)$. Because $h = 0$, the bilinear form $((v, u))$ has the form (2.11).

Let us start by proving that the domain Ω has a Lipschitz continuous boundary. To do that, according to Def. 28.6 in [14], we have to prove that there exist constants $\alpha > 0$, $\beta > 0$, a finite number m of Cartesian coordinate systems x_1^r, x_2^r, $r = 1, ..., m$, and m functions $a_r(x_1^r)$ continuous in the interval $[-\alpha, \alpha]$ satisfying certain properties. In particular, every point of the boundary has to be expressed as

$$x = [x_1^r, a_r(x_1^r)], \tag{2.21}$$

for at least one $r = 1, ..., m$. Moreover, the points $x = (x_1^r, x_2^r)$ such that

$$|x_1^r| < \alpha, \tag{2.22}$$

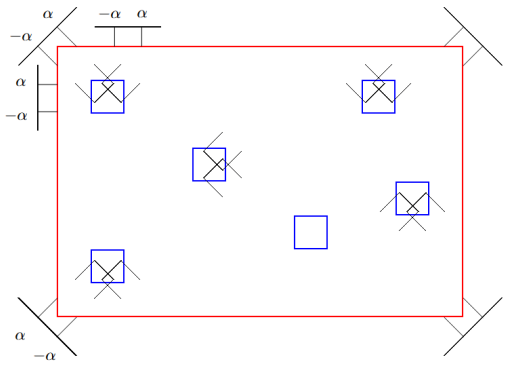

FIG. 2.2. *Cartesian coordinates systems for the domain Ω such that every point on $\partial\Omega$ can be expressed in the form $[x_1^r, a_r(x_1^r)]$.*

lie in Ω or outside $\bar{\Omega}$, i.e.

$$a_r(x_1^r) < x_2^r < a_r(x_1^r) + \beta \tag{2.23}$$

or

$$a_r(x_1^r) - \beta < x_2^r < a_r(x_1^r). \tag{2.24}$$

Finally, the functions $a_r(x_1^r)$, $r = 1, ..., m$ have to satisfy the Lipschitz condition on $[-\alpha, \alpha]$.

Then, let us first define the Cartesian coordinates systems for our domain as depicted in Fig 2.2. We choose $\frac{k\sqrt{2}}{4} < \alpha < \frac{k\sqrt{2}}{2}$. Remind that, to define the model problem, we divided the pixel square into 9 smaller squares and selected the central one. Therefore, k is the measure of the side of the small square. For the inner squares, we choose the Cartesian coordinates systems on the diagonals of the squares. Therefore, we have 4 Cartesian coordinate systems, 2 for each diagonal, covering the entire boundary of the square. This particular choice of α is due to the inner squares: indeed, the limit value $\frac{k\sqrt{2}}{4}$ is half of the length of the segment obtained connecting the middle points of the sides. If $\alpha \leq \frac{k\sqrt{2}}{4}$, there will be some points in the sides that are not expressed by any Cartesian coordinate system. On the other side, if $\alpha \geq \frac{k\sqrt{2}}{2}$, we would not be able to find any β satisfying the required conditions (2.23) or (2.24). Having defined the 4 Cartesian coordinate systems for one inner square, each point on the boundary of the square can be expressed as

$$[x_1^r, a_r(x_1^r)] \tag{2.25}$$

with

$$a_r(x_1^r) = C - |x_1^r|, \tag{2.26}$$

where $C = \frac{k\sqrt{2}}{2} - \alpha$ is a constant. This construction is applied to every inner square. For the outer rectangle, we define the Cartesian coordinate systems in a similar way. In this case, we define 4 coordinate systems perpendicular to one of the diagonals of the rectangle to express the points around the corners ($\alpha > 0$ is already fixed). We

then add $2(\lfloor \frac{L_1}{2\alpha} \rfloor + \lfloor \frac{L_2}{2\alpha} \rfloor)$ Cartesian coordinate systems parallel to the rectangle sides L_1 and L_2 to cover the other points. Therefore, each point in Γ^2 can be expressed as

$$[x_1^r, a_r(x_1^r)] \tag{2.27}$$

with

$$a_r(x_1^r) = |x_1^r| + C, \tag{2.28}$$

and

$$a_r(x_1^r) = C. \tag{2.29}$$

We then choose $\beta < C$ to ensure that conditions (2.23) and (2.24) are satisfied for the inner squares; the conditions automatically hold also for the outer rectangle. Finally, we have to prove that the functions $a_r(x_1^r)$, satisfy the Lipschitz condition, therefore that $\forall r$ exists $L_r > 0$ such that for all x, y in the interval $[-\alpha, \alpha]$ in the Cartesian coordinate system x_1^r, x_2^r it holds

$$|a_r(x) - a_r(y)| \leq L_r |x - y|. \tag{2.30}$$

For (2.26) and (2.28), we choose $L_r = 1$, and the condition (2.30) follows from the reverse triangle inequality. For (2.29), we can choose any $L_r > 0$.
Therefore, Ω has a Lipschitz continuous boundary. Condition (2.14) is satisfied because, on each square, the Dirichlet conditions are constant. The proof of the V-ellipticity of the bilinear form (2.11) follows from Theorem 30.3 in [14], and Theorem 1.9 in [12]; indeed for $v \in V$ there exists $C_1 > 0$ such that

$$\|v\|_V^2 = \|v\|_{W_2^1(\Omega)}^2 \leq C_1 \left(\int_{\Gamma^1} |v|^2 dS + \int_\Omega \left| \frac{\partial v}{\partial x_1} \right|^2 + \left| \frac{\partial v}{\partial x_2} \right|^2 dx \right) = C_1((v, v)), \tag{2.31}$$

where $\int_{\Gamma^1} |v|^2 dS = 0$ because $v \in V$. Hence, choosing $\mu = \frac{1}{C_1}$ we obtain (2.19). The boundedness of the bilinear form (2.11) follows from Schwarz inequality [14].
Finally, we need to prove that there exists $w \in W_2^1(\Omega)$ satisfying (2.16). To do that, consider a square grid in Ω with size k so that the squares $S_p(k)$ will be squares of the grid. Consider a discretization of the following boundary value problem

$$\begin{cases} -\Delta u(x) = 0, & x \in \Omega, \\ u(x) = 0, & x \in \Gamma^2, \\ u(x) = g(x), & x \in \Gamma^1. \end{cases} \tag{2.32}$$

We consider the values $u_{i,j}$, $i = 1, ..., n_1$, $j = 1, ..., n_2$ on the vertices of the squares of the grid, see Fig. 2.3. Hence, the Dirichlet boundary conditions are prescribed on the vertices of the squares $S_p(k)$. Let us indicate by v_p the constant value on Γ_p^1, $p = 1, ..., s$. The discretization of (2.32) by finite differences method is then given as follows:

$$\begin{cases} u_{i,j} = 0, & \text{on } \Gamma^2, \\ u_{i,j} = v_p, & \text{on } \Gamma_{\mathrm{p}}^1,\ \mathrm{p} = 1, ..., \mathrm{s}, \\ -u_{i-1,j} - u_{i,j-1} + 4u_{i,j} - u_{i+1,j} - u_{i,j+1} = 0, & \text{for other vertices.} \end{cases} \tag{2.33}$$

We will prove that the matrix A with elements $A_{i,j}$ representing the discrete system of equations (2.33) is weakly chained diagonally dominant (WCDD) [2]. Then,

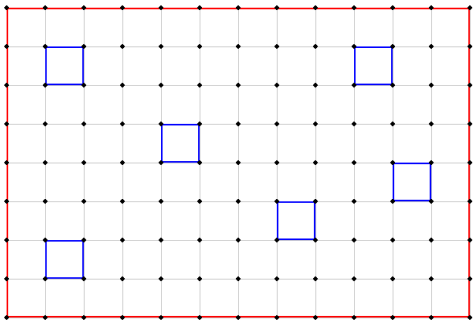

FIG. 2.3. *Discretization of the domain Ω for the boundary value problem (2.32). The grid nodes are prescribed on the vertices of the squares.*

we will know that it is not singular; thus, a unique solution exists. Indeed, A is weakly diagonally dominant (WDD), i.e., $|A_{i,i}| \geq \sum_{i \neq j} |A_{i,j}|$. To prove that A is WCDD, we consider the directed graph associated with the matrix A defined as follows: the vertices of the graph are the rows of the matrix A, and there exists an edge $i \to j$ if and only if $A_{i,j} \neq 0$.
The matrix A is composed of blocks of strictly diagonally dominant (SDD) rows, i.e. $|A_{i,i}| > \sum_{i \neq j} |A_{i,j}|$, and blocks of WDD rows; one possible realization of A is depicted in (2.34). Notice that the SDD rows are related to the Dirichlet boundary conditions in (2.33), where we have 1 on the diagonal and 0 everywhere else.

$$
\begin{array}{c}
\\
\\
\\
i-1 \\
i \\
i+1 \\
\\
\\
\\
\\
\\
\\
\\
\\
\end{array}
\begin{pmatrix}
1 & 0 & \cdots & \cdots & \cdots & 0 & \cdots & \cdots & \cdots & 0 & 0 & 0 \\
 & \ddots & & & & \ddots & & & & \ddots & & \\
 & & \ddots & & & \ddots & \ddots & & & & & \\
0 & \cdots & 0 & 1 & 0 & & \cdots & & \cdots & & & 0 \\
\vdots & & & & & & & & & & & \\
0 & -1 & \cdots & -1 & 4 & -1 & \cdots & -1 & \cdots & \cdots & 0 & 0 \\
0 & \cdots & -1 & \ldots & -1 & 4 & -1 & \ldots & -1 & 0 & 0 & 0 \\
 & & \ddots & & & & \ddots & & & \ddots & & \vdots \\
 & & & & & \ddots & & \ddots & & & \ddots & \\
 & & \ddots & & & & \ddots & & \ddots & & & \\
 & & & & & & & & & \ddots & & \\
\vdots & & \ddots & & \ddots & & & \ddots & & \ddots & \ddots & \\
0 & \cdots & \cdots & \cdots & \cdots & 0 & \cdots & \cdots & \cdots & 0 & 0 & 1
\end{pmatrix}
\tag{2.34}
$$

We have to prove that, starting from each WDD row, a walk in the directed graph ends at an SDD row. To do that, let us first assume that the row i is WDD, and the row $i-1$ is *SDD*. For the i-th row we have $A_{i,i-1} = -1 \neq 0$, therefore in the directed graph we will have $i \to i-1$. A more general case is depicted in Fig. 2.4, which corresponds to the graph of the matrix A depicted in (2.34) for the rows $i-1$, i, and $i+1$. In this case, the rows i and $i+1$ are WDD, while the row i is SDD. Since between two consecutive WDD rows, it always holds $A_{i,i+1} \neq 0$ and $A_{i+1,i} \neq 0$, we will always be able to find a walk ending at an SDD row. Then, we proved that the

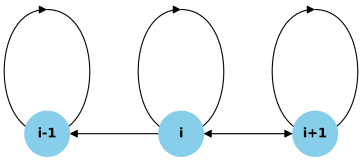

FIG. 2.4. *Graph of the matrix A depicted in (2.34) for the rows $i-1$, i, and $i+1$*

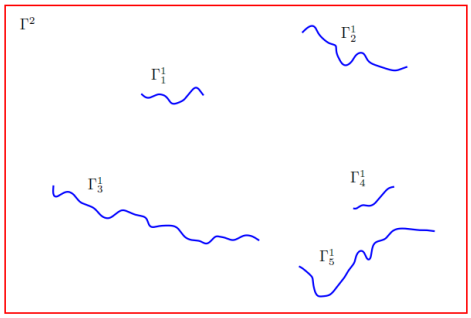

FIG. 2.5. *Example of open set Ω bounded by open curves Γ_p^1 and closed curve Γ^2*

matrix A is WCDD and, therefore, non-singular.
Let us indicate by U the solution of (2.33). To define w from Def. 2.1, we consider the bilinear interpolation of U on the grid, and we obtain a function defined on Ω satisfying the prescribed Dirichlet boundary conditions on Γ^1. The function w is continuous with piecewise continuous derivatives, therefore $w \in W_1^2(\Omega)$. This concludes the proof. □

REMARK 1. *Let us now consider another approach to define the model problem. To consider the minimization problem in equation (1.1), we first have to define the domain Ω bounded by the boundary of $\tilde{\Omega}$ and by open curves; an example is depicted in Fig. 2.5.*

Let us denote by Γ_p^1, $p = 1, 2, ..., s_d$ the inner open curves. Set

$$\Gamma^1 = \bigcup_{p=1}^{s_d} \Gamma_p^1, \qquad \Omega = \tilde{\Omega}/\Gamma^1, \tag{2.35}$$

so that

$$\partial\Omega = \Gamma^2 \cup \Gamma^1. \tag{2.36}$$

We solve the minimization problem in Ω subject to the following boundary conditions

- *Zero Neumann boundary conditions on the domain boundary*

$$\frac{\partial u}{\partial \nu}(x) = 0 \qquad x \in \Gamma^2, \tag{2.37}$$

where ν is the unit outer normal vector to the boundary Γ^2.

- *Dirichlet boundary conditions on the inner open curves*

$$u(x) = g(x) \qquad x \in \Gamma^1, \tag{2.38}$$

where $g : \Gamma^1 \to \mathbb{R}$ is a function that returns the values given by sparse samples. Solving the variational problem (1.1) with conditions (2.37) and (2.38) is equivalent to finding the solution of the following boundary value problem

$$\begin{cases} -\Delta u(x) = 0, & x \in \Omega, \\ \frac{\partial u}{\partial \nu}(x) = 0, & x \in \Gamma^2, \\ u(x) = g(x), & x \in \Gamma^1. \end{cases} \tag{2.39}$$

It can be proved that, under suitable assumptions on Γ^1_p and Γ^2, the classical solution of (2.39) exists and is unique [7]. In particular, Γ^2 has to be of class C^2. Moreover, $\forall p = 1, .., s$, we require Γ^1_p to be a non-closed smooth arc of finite length without self-intersections of class $C^{2,\lambda}$, $\lambda \in (0, 1]$. Here, $C^{2,\lambda}$ indicates the set of curves belonging to the class C^2 and such that the second derivatives of the coordinate functions are Hölder continuous with exponent λ. Since we did not study the regularity of the curves representing the smoothed trajectories obtained by our model presented in [9], we can not use theory from [7] directly. Therefore, starting from our trajectories, we construct quartic splines as in [3]. These splines are of class C^3, satisfying the required continuity conditions. If we understand the second approach in a discrete way, the velocities given in discrete points can be understood as sparse samples, and we can use the first approach.

3. Numerical experiments. For the numerical experiments, we use the discretization from [10], which is slightly different from the one used in the proof of theorem in the previous section. In system (2.33), we considered the grid points in the corners of the squares of side k to discretize the Laplace equation. Here, we consider the mean value in the center of the squares. Since the Dirichlet conditions are constant on each square, the mean value is the same constant.

For the discretization, we consider the uniform squared grid $N_1 \times N_2$, where N_1 is the height, N_2 is the width of the grid with size $k = 1$. We use the finite difference method: the grid nodes correspond to the centers of the squares. We use the 5 points approximation to discretize the Laplace operator and the reflection of values along the boundary to approximate the zero Neumann boundary condition, for details see [10]. We obtain a linear system as in [10] and solve it using the Bi-conjugate gradient stabilized algorithm from Eigen::BiCGSTAB class of [6].

We first performed some numerical tests, as shown in Figs. 3.1, 3.2. In Fig. 3.1, the prescribed Dirichlet conditions are vectors on parallel lines with the length of the vector set as constant on the line. The vectors were normalized for better visualization: the color represents the norm. The direction of the vectors in the reconstructed vector field is extrapolated from the two parallel lines in the direction to the boundary; therefore, it remains constant. The vector length changes linearly from the smallest to the biggest value between the two parallel lines and is extrapolated where the vectors are not influencing each other. In Fig. 3.2, the prescribed Dirichlet conditions are vectors on 2 lines: the direction and the length are fixed on the line, but it is different between the lines. We observe that the vectors in the reconstructed vector field smoothly change direction and length in the regions influencing each other. On the other hand, both the direction and the length are extrapolated from the Dirichlet

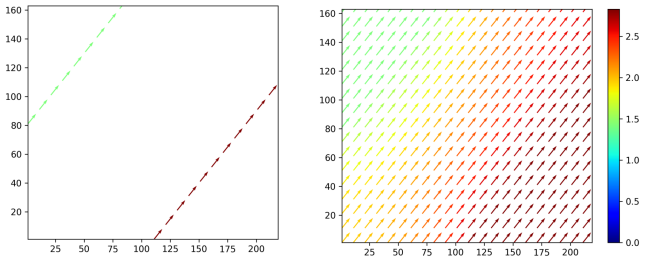

FIG. 3.1. *Left: prescribed Dirichlet condition. Right: vector field reconstruction by triple-Laplacian*

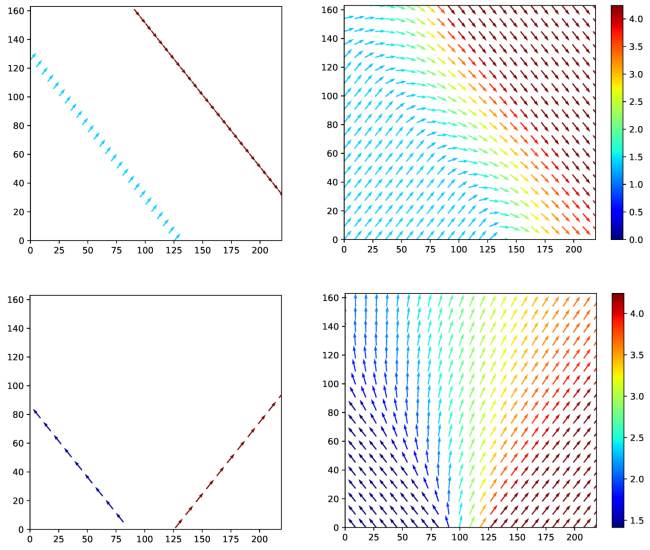

FIG. 3.2. *Left: prescribed Dirichlet condition. Right: vector field reconstruction by triple-Laplacian*

conditions where the vectors do not influence each other.

To better understand the reason why we use the triple-Laplacian model, we selected the simple case of two vectors with the same length but different directions as shown in Fig. 3.3. If only the double-Laplacian is used, the interpolation between the vectors will give shorter vectors smoothly changing direction from one Dirichlet condition to the other, as shown on the bottom right of Fig. 3.3. When we compute the triple-Laplacian, the result of the reconstruction extrapolates the lengths from the given ones; therefore, the length of the vectors in the reconstructed vector field by triple-Laplacian is constant everywhere as shown on the bottom left of Fig. 3.3. Again, we do not add/create any new information that is not contained in Dirichlet conditions.

To evaluate the quality of the reconstruction of our model, we considered the following experiment. We defined 2 vector fields in $[-1,1] \times [-1,1]$: the expansion

$$V(x_1, x_2) = (x_1, x_2), \tag{3.1}$$

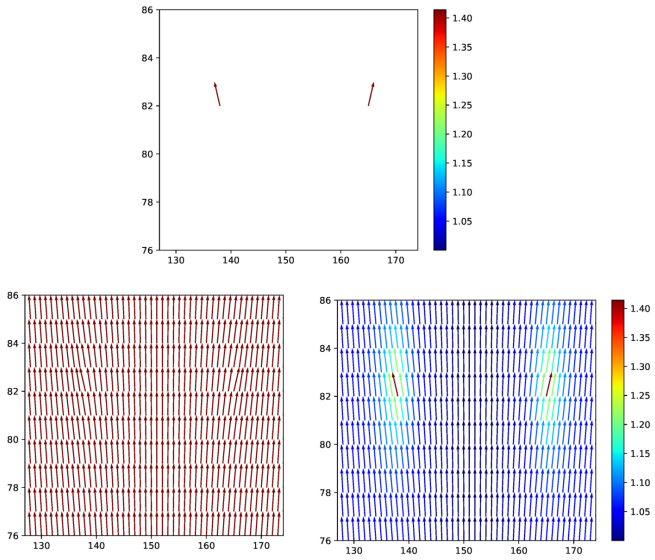

FIG. 3.3. *Top: prescribed Dirichlet condition. Bottom left: vector field reconstruction by triple-Laplacian. Bottom right: vector field reconstruction by double-Laplacian*

and the rotation

$$V(x_1, x_2) = (-x_2, x_1). \tag{3.2}$$

We fixed a percentage of pixel values for each experiment to keep: these pixels are randomly selected, and the random selection is done 5 times. Then, we reconstructed the vector field using triple-Laplacian with the given samples. We calculated the root mean squared error (RMSE) between the reconstructed vector field and the original one, namely

$$\|V_R - V_E\|_{L_2} = \sqrt{\frac{1}{n}\sum_{i=1}^{n}\|V_R(x_1^i, x_2^i) - V_E(x_1^i, x_2^i)\|^2}, \tag{3.3}$$

where n is the number of pixels that have been reconstructed. Then, we computed the mean of the RMSE of the 5 different random pixel selections. In Fig. 3.4, we show the results for the vector fields defined in (3.1) and (3.2). We plotted the RMSE against the percentage of pixels kept for the reconstruction. The error decreases for an increasing percentage of kept pixels; indeed, the prescribed Dirichlet conditions are closer to each other, making the interpolation process more precise. Tab. 3.1 shows the computed RMSE for increasing percentages of kept pixels. In both cases, the reconstruction of the vector field for at least 30% of kept pixels (that is, the percentage of sparse samples with respect to the total number of points) is less than 10^{-3}.

Then, we reconstructed the velocity vector field caused by the danger signals and driving the macrophages toward the wound. The trajectories were extracted with the algorithm described in [13] and smoothed with the model described in [9]. The smoothing algorithm allows us to find the velocity vectors on the smoothed curves:

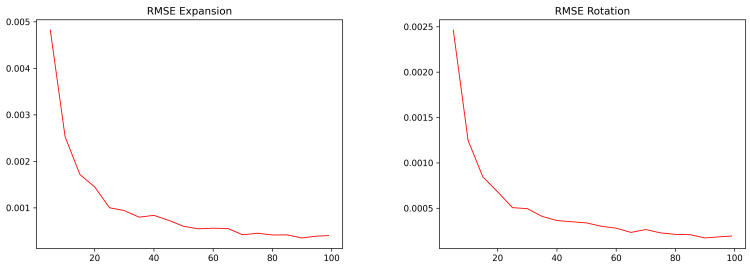

FIG. 3.4. *Left: RMSE for the vector field in Eq. (3.1). Right: RMSE for the vector field in Eq. (3.2).*

TABLE 3.1
RMSE for increasing percentage of kept pixels for expansion (3.1) and rotation (3.2).

% of points as DBC	RMSE Expansion	RMSE Rotation
10	2.528425e-003	1.245681e-003
20	1.448192e-003	6.784626e-004
30	9.404206e-004	4.941736e-004
40	8.377425e-004	3.628637e-004
50	6.026122e-004	3.370405e-004
60	5.621018e-004	2.788309e-004
70	4.203156e-004	2.637498e-004
80	4.161753e-004	2.109483e-004
90	3.523628e-004	1.713661e-004

we use these vectors as prescribed Dirichlet conditions. Fig. 3.5 shows the smoothed velocity vectors found smoothing macrophage trajectories and the corresponding reconstructed velocity vector field.

4. Discussion and Conclusion. In this paper, we solved the problem of reconstructing a vector field from sparse samples. We solved a minimization problem by considering the sparse samples as prescribed Dirichlet conditions inside the domain. Minimizing the Dirichlet energy is equivalent to finding the Laplace equation's solution with prescribed boundary conditions. We imposed zero Neumann boundary conditions on the domain's boundary so as not to add any new information not already given by the sparse samples. We used the proposed model to reconstruct the velocity vector field caused by the danger signals and driving macrophages toward the wound during wound healing. We extracted the trajectories and smoothed them to separate the directional parts of motion from the random parts. We found the velocity vectors on the smoothed curve and considered them as prescribed Dirichlet conditions to reconstruct the vector field. The velocity vector field considered in this paper is stationary. One possible improvement would be to consider a time-dependent vector field and apply the same mathematical model to reconstruct the vector field. The existence of a weak solution when the squares touch each other is another possible generalization of the theoretical formulation of the problem. Indeed, in that case, the domain is no longer Lipschitz. Moreover, one can study the existence of a solution when the Dirichlet conditions are given in points. Finally, the overall workflow can be straightforwardly extended in 3D.

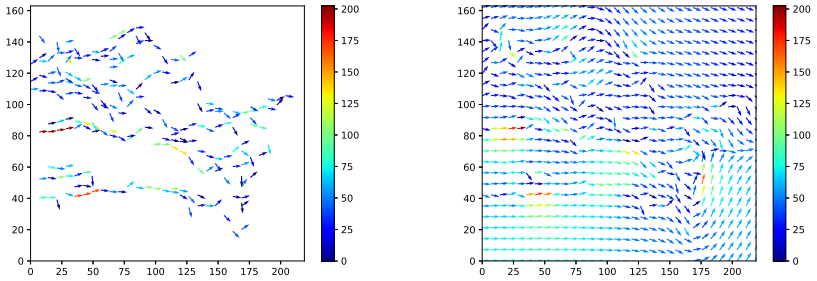

FIG. 3.5. *Left: prescribed Dirichlet condition. Right: vector field reconstruction by triple-Laplacian*

5. Acknowledgement. This work was supported by grants APVV-19-0460, APVV-23-0186, VEGA 1/0249/24 and EC project INFLANET.

REFERENCES

[1] Ahlfors, L.V.: Complex analysis : an introduction to the theory of analytic functions of one complex variable. McGraw-Hill (1979)
[2] Azimzadeh, P., Forsyth, P.A.: Weakly chained matrices, policy iteration, and impulse control. SIAM Journal on Numerical Analysis **54**(3) (2016)
[3] Banchs, R.: Natural quartic splines. Research progress report no. 7 on Time Harmonic Field Electric Logging, University of Texas at Austin (1996), `https://rbanchs.com/publications/reports.html`
[4] Belhachmi, Z., Bucur, D., Burgeth, B., Weickert, J.: How to choose interpolation data in images. SIAM Journal on Applied Mathematics **70**(1) (2009)
[5] Fisher, M., Schröder, P., Desbrun, M., Hoppe, H.: Design of tangent vector fields. ACM Transactions on Graphics (TOG) **26**(3) (2007)
[6] Gaël, G., Benoît, J., et al.: Eigen v3. `http://eigen.tuxfamily.org` (2010)
[7] Krutitskii, P.: The mixed harmonic problem in a bounded cracked domain with dirichlet condition on cracks. Journal of Differential Equations **198**(2) (2004)
[8] Lage, M., Petronetto, F., Paiva, A., Lopes, H., Lewiner, T., Tavares, G.: Vector field reconstruction from sparse samples with applications. 19th Brazilian Symposium on Computer Graphics and Image Processing (2006)
[9] Lupi, G., Mikula, K., Park, S.A.: Macrophages trajectories smoothing by evolving curves. Tatra Mountains Mathematical Publications **86**(1) (2023)
[10] Mikula, K., Ambroz, M., Mokošová, R.: What was the river ister in the time of strabo? a mathematical approach. Tatra Mountains Mathematical Publications **80**(3) (2021)
[11] Mussa-Ivaldi, F.: From basis functions to basis fields: vector field approximation from sparse data. Biological Cybernetics **67** (1992)
[12] Nečas, J.: Direct methods in the theory of elliptic equations. Springer Berlin, Heidelberg (2012)
[13] Park, S.A., Sipka, T., Krivá, Z., Nguyen-Chi, M., Lutfalla, G., Mikula, K.: Segmentation-based tracking of macrophages in 2d+time microscopy movies inside a living animal. Computers in Biology and Medicine **153** (2022)
[14] Rektorys, K.: Variational Methods in Mathematics, Science and Engineering. Springer Netherlands (2012)
[15] Schönlieb, C.B.: Partial Differential Equation Methods for Image Inpainting. Cambridge University Press (2015)
[16] Sipka, T., Peroceschi, R., Groß, M., Ellett, F., Pescia, C., Gonzalez, C., Lutfalla, G., Nguyen-Chi, M.: Damage-induced calcium signaling and reactive oxygen species mediate macrophage activation in zebrafish. Frontiers in Immunology **12** (2021)